CHINA FOUNDRY Research & Development
Vol. 21 No. 2 March 2024
www.springer.com/41230
https://doi.org/10.1007/s41230-024-3088-8

Oxidation behavior of 4774DD1 Ni-based single-crystal superalloy at 980 °C in air

Yu Fang[1], Ya-zhou Li[2], *Qiang Yang[2], **Qun-gong He[1], Xiu-fang Gong[1], Qian Duan[2], Hai-yang Song[2], Fu Wang[2], Qiong-yuan Zhang[1], and Hong Zeng[1]

1. State Key Laboratory of Long-Life High Temperature Materials, Dongfang Turbine Co., Ltd., Deyang 618000, Sichuan, China

2. State Key Laboratory for Manufacturing System Engineering, School of Mechanical Engineering, Xi'an Jiaotong University, Xi'an 710049, China

Abstract: The oxidation behavior of a novel Ni-based single-crystal 4774DD1 superalloy for industrial gas turbine applications was investigated by the isothermal oxidation at 980 ºC and discontinuous oxidation weight gain methods. The phase constitution and morphology of surface oxides and the characteristics of the cross-section oxide film were analyzed by XRD, SEM and EDS. Results show that the oxidation kinetics of the 4774DD1 superalloy follows the cubic law, indicating its weak oxidation resistance at this temperature. As the oxidation time increases, the composition of the oxide film evolves as following: One layer consisting of a bottom Al_2O_3 sublayer and an upper (Al_2O_3+NiO) mixture sublayer after oxidized for 25 h. Then, two layers composed of an outermost small NiO discontinuous grain layer and an internal layer for 75 h. This internal layer is consisted of the bottom Al_2O_3 sublayer, an intermediate narrow $CrTaO_4$ sublayer, and an upper (Al_2O_3+NiO) mixture sublayer. Also two layers comprising an outermost relative continuous NiO layer with large grain size and an internal layer as the oxidation time increases to 125 h. This internal layer is composed of the upper (Al_2O_3+NiO) mixture sublayer, an intermediate continuous ($CrTaO_4$+$NiWO_4$) mixture sublayer, and a bottom Al_2O_3 sublayer. Finally, three layers consisting of an outermost ($NiAl_2O_4$+$NiCr_2O_4$) mixture layer, an intermediate ($CrTaO_4$+$NiWO_4$) mixture layer, and a bottom Al_2O_3 layer for 200 h.

Keywords: nickel-base single crystal superalloy; oxidation kinetics; oxide film; microstructure; mechanism

CLC numbers: TG146.1+5 **Document code:** A **Article ID:** 1672-6421(2024)02-116-09

1 Introduction

Ni-based single-crystal superalloys have been extensively utilized in aero-engines for the production of hot-end components due to their excellent high-temperature mechanical properties [1-4]. In the pursuit of heightened thermal efficiency, single-crystal superalloys are progressively being introduced into industrial gas turbines (IGTs) [5-7] to fabricate single-crystal blades, thereby enhancing the turbine front-end temperature. Although the blades are generally used in coated condition and the thermal barrier coatings can improve the oxidation resistance, the oxidation behavior of the base superalloy is very important in the event that the thermal barrier coating is failure. When the coating is damaged, the base superalloy will be exposed to oxygen-containing atmosphere. Due to the extremely harsh service environment of IGTs, such as the high temperature, high thermal shocking and high cycling load, the oxidation of superalloy can result in initiation and propagation of cracks in single-crystal blades, significantly reducing the service life of IGTs [8-10]. Therefore, it is imperative to thoroughly investigate the intrinsic behavior of base single-crystal superalloy in oxidizing atmosphere.

Long-time exposure at high temperature is a conventional measurement method used to study the oxidation behavior of single-crystal superalloy. It is important to investigate the characteristics of oxidation kinetics, including changes in mass over time, as well as the chemical composition and microstructure of the oxide film. Numerous studies have been conducted in these areas over the past few decades. Pei et al. [11] reported that the oxidation kinetics of DD6 Ni-based

***Qiang Yang**

Male, born in 1987, Ph. D., Associate Researcher, a Senior Member of Chinese Mechanical Engineering Society. His research interests mainly focus on additive manufacturing and preparation of single crystal turbine blades.

E-mail: qiangyang@xjtu.edu.cn

****Qun-gong He**

E-mail: hequngong@dongfang.com

Received: 2023-07-21; Accepted: 2023-11-22

single crystal superalloy at temperatures of 1,050 °C and 1,100 °C followed the parabolic law. The oxide film primarily consisted of $NiTa_2O_6$, $CoCo_2O_4$, $CoWO_4$, $NiCr_2O_4$ and other complex compounds and spinel phases, as well as continuous α-Al_2O_3. Zhou et al. [12] found that the oxidation kinetics of a new Re-free Ni-based single crystal superalloy at 950 °C approximately obeyed parabolic law. Its oxide film consisted of NiO, CoO, Cr_2O_3, Al_2O_3 and a small amount of spinel compounds such as $CrTaO_4$, $NiCr_2O_4$, $CoCrAl_2O_4$, $CoAl_2O_4$ and $NiAl_2O_4$. A study of Shi et al. [13] showed that the oxidation kinetics of single-crystal DD6 alloy obeyed subparabolic rate law during oxidation of 100 h at 1,050 °C and 1,100 °C. The oxide scale was made up of NiO, Al_2O_3, Cr_2O_3 and TaO_2. Liu et al. [14] reported that the oxidation kinetics of single-crystal DD32 superalloy at 900 °C and 1,000 °C obeyed a parabolic law at the initial state, and the asymptotic level linear law at the second steady state stage. The oxide scale was composed of NiO, CoO, $W_{20}O_{58}$, $CrTaO_4$, $NiCr_2O_4$, $NiAl_2O_4$, $CoAl_2O_4$ and α-Al_2O_3. Hu et al. [15] found that the oxidation behavior of a Ni-based single-crystal superalloy over the temperature range of 850 °C–950 °C followed an approximate power law. The oxide film comprised NiO, $NiCr_2O_4$, $CrTaO_4$, and Al_2O_3. Li et al. [16] found that under different oxygen concentrations at 1,100 °C, the oxidation kinetics of nickel-based single crystal superalloy basically conformed to the parabolic law, but the microstructure of the oxide scale was changed. Hu et al. [17] reported that the oxidation kinetics of DD6 single-crystal superalloy at 980 °C was not rigorously followed the parabolic law in the whole oxidation process, while it could be divided into two stages: the Al_2O_3 and NiO were formed in the initial stage, and the complex spinel phases of $NiCrO_4$, $NiAl_2O_4$, $CrTaO_4$ and CoO were formed in the steady stage. Moreover, some studies also found that a γ'-free zone (Al depletion zone) formed between the oxide layer and the single-crystal Ni-based superalloy matrix due to the diffusion of Al elements after oxidation [15,18]. All these studies indicate that the chemical composition, the oxidizing temperature and oxidizing conditions have a great effect on the oxidation behavior of Ni-based single-crystal superalloys.

4774DD1 is a novel Ni-based single-crystal superalloy developed by Dongfang Turbine Co., Ltd., Deyang, China. It is used for casting IGTs single-crystal blades and exhibits an excellent high-temperature mechanical property. In this study, the long-time isothermal oxidation behaviors and mechanisms of 4774DD1 single-crystal superalloy exposed at 980 °C (a typical servicing temperature of blades surface in IGTs) for 200 h, were investigated in detail, including the oxidation kinetics, microstructure and chemical composition of oxide films. The results can provide a theoretical basis for the engineering application of 4774DD1 single-crystal blades in IGTs, and have a significant value for the design and development of single-crystal blades for gas turbines.

2 Experimental procedure

4774DD1 Ni-based single-crystal superalloy (Dongfang Turbine Co., Ltd., Deyang, China) was employed as raw material. Its chemical composition is listed in Table 1. The directional solidification processes were as follows: Firstly, melting the alloy in a crucible which was positioned in the induction melting coil. Then, fixing the investment mold cluster onto the chill plate and raising it into a mold-heater. A vacuum of 1×10^{-3} Pa would be achieved in the furnace chamber before preheating the mold to 1,500 °C. Then, the molten alloy at 1,500 °C was poured into the mold, and finally the single-crystal bars were obtained under a withdrawal speed of 3 mm·min^{-1}. The [001] orientated single-crystal samples of 8 mm×8 mm×7.5 mm in size were cut from the 4774DD1 single-crystal bars. The surface of the samples was then polished using a combination of grinding papers ranging from 300 to 1,000 grit and then by diamond-based polishing solutions ranging from 9 μm to 0.05 μm, and washed in ethanol by using ultrasonic cleaning. The isothermal oxidation was conducted in a high-temperature box furnace (KSL-1200X, Shenyang Kejing Auto-Instrument Co., Ltd., Shenyang, China) at 980 °C. To achieve the profiles of oxidation kinetics, the weight change of the samples after taken out of the furnace was measured every 25 h using an electronic analytical balance [ME204, Mettler Toledo Technology (China) Co., Ltd.] with an accuracy of 0.1 mg. The total oxidizing period was 200 h. The microstructure, chemical composition and phase constitution of oxidation films were analyzed by using scanning electron microscopy (SEM) (Zeiss Sigma300, Carl Zeiss AG, Oberkochen, Germany) equiped with an energy dispersive X-ray spectroscopy (EDS), and X-ray diffraction (XRD) (D8 Advance, Bruker AXS GmbH, Karlsruhe, Germany).

Table 1: Chemical composition of 4774DD1 alloy (wt.%)

Cr	Co	Mo	W	Ta	Hf	Al	Ti	Re	Ni
6.4%	9.6%	0.6%	6.5%	6.4%	0.1%	5.5%	1.0%	3.0%	Bal.

3 Results and discussion

3.1 Oxidation kinetics of 4774DD1 alloy

Figure 1 shows the oxidation kinetic curves, i.e., curves of mass gain per unit area, $\Delta m/A$ (Δm is mass gain of sample before and after oxidation test; A is original surface area of sample), vs. oxidation time (t) of the alloy at 980 °C. It can be seen that the mass gain increases obviously as a function of oxidation time. At the beginning of exposure time of 25 h, the rate of mass gain is very fast, while it decreases with the extension of exposure time. When the exposure time exceeds 175 h, the rate of mass grain is approximately equal to zero.

The relationship between mass change (Δm) and exposure time (t) during oxidation generally follows a power law [19], as

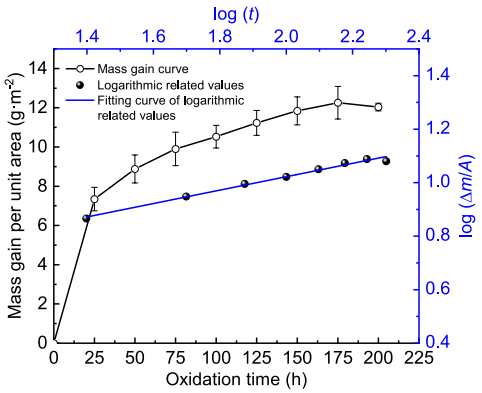

Fig. 1: Oxidation kinetic curve of the alloy at 980 °C: mass gain per unit area versus exposure time and the logarithmic relation curve

follows:

$$\frac{\Delta m}{A} = kt^n + C \tag{1}$$

where k refers to an oxidation rate constant; n denotes reaction order; C is a constant and negligible. Logarithms is taken on both sides of the equation, then

$$\log(\frac{\Delta m}{A}) = n\log(t) + \log k \tag{2}$$

The logarithmic relation curve, log($\Delta m/A$) vs. log(t), of the alloy at 980 °C can be obtained by linear fitting of the mass gain data with Eq. (2), which approximately conforms to a straight-line law, as shown in Fig. 1. The slope of the line is the reaction order n. It is found that the reaction order n of the alloy at 980 °C is approximately 0.25, thus the oxidation kinetic can be inferred to obey the cubic law, which is consistent with previous study [20]. The intercept is the log value of the oxidation rate constant k; for alloy 4774DD1, k is calculated to be 3.32109 $g^n \cdot (m^{2n} \cdot h)^{-1}$ accoring to Eq. (2) and Fig. 1.

$\overline{K^+}$ is the average oxidation rate of the alloy, and

$$\overline{K^+} = \frac{\Delta \overline{m}}{A \cdot t} \tag{3}$$

where $\Delta \overline{m}$ is the average mass gain of sample before and after oxidation. The average oxidation rate of 4774DD1 alloy with different oxidation times (t) can be obtained according to Eq. (3), as shown in Fig. 2. Generally, the average oxidation rate of the alloy can be used to evaluate the oxidation resistance of alloys. When the $\overline{K^+}$ is less than 0.1, it indicates that the alloy reaches the level of complete oxidation resistance. When the $\overline{K^+}$ is greater than 0.1, but less than 1, it indicates that the alloy reaches the level of oxidation resistance. These two levels of oxidation resistance indicates that the superalloy possesses good oxidation resistance and can be utilized for manufacturing of the single-crystal blades for IGTs [21]. The average oxidation rate of the 4774DD1 alloy is 0.1–0.3 $g \cdot m^{-2} \cdot h^{-1}$ from 0 h to 100 h, and less than 0.1 $g \cdot m^{-2} \cdot h^{-1}$ from 100 h to 200 h, indicating that the alloy exhibits a certain degree of oxidation resistance at 980 °C, which is consistent with the Ref. [19].

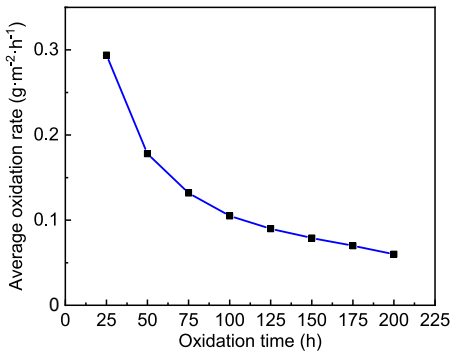

Fig. 2: Average oxidation rate of the alloy at 980 °C

3.2 Oxides analysis on surface

Figure 3 shows the XRD analysis results performed on the surface of the samples to determine the oxidation products formed at 980 °C after exposured for 25 h, 75 h, 125 h, and 200 h. Since this analysis is performed on the surface, the actual oxidation products might not be completely identified. After the samples oxidated for 25 h, the oxidation products are mainly Al_2O_3 with a small amount of NiO combined with the EDS results in Fig. 4. With prolonging exposure time to 75 h, the primary oxides are Al_2O_3, NiO and a little of $CrTaO_4$. With further increasing exposure time to 125 h, the products formed are mainly composed of Al_2O_3, NiO, $CrTaO_4$ and some $NiWO_4$. After oxidation for 200 h, the oxidation products principally consist of $NiAl_2O_4$, $NiCr_2O_4$, $CrTaO_4$, $NiWO_4$ and Al_2O_3.

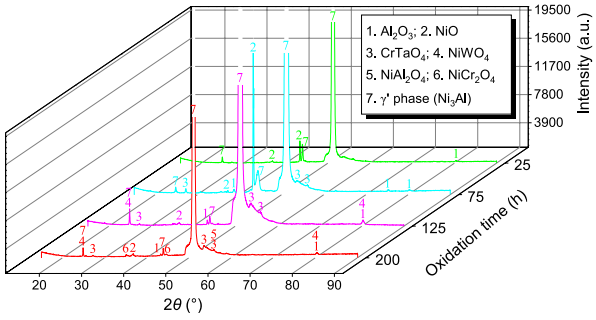

Fig. 3: XRD phases analysis of sample surface after oxidation at 980 °C for different exposure times

3.3 Morphologies of cross-section oxide film

Figure 4 shows the cross-sectional morphology and EDS mapping results of the oxide film of the alloy oxidized at 980 °C for 25 h. As shown in Fig. 4(a), a thin oxide film is formed on the surface of the sample. Table 2 lists the EDS analysis results of two interesting positions marked in Fig. 4(a). According to the aluminum (Al) element map in Fig. 4(b) and the EDS point analysis results in Table 2, Al element greatly concentrates in the film. Figure 4(c) illustrates that some nickel (Ni) element concentrates in the upper parts of the film, which is further proved by the EDS analysis of Position 1 in Fig. 4(a). No obvious concentration of other alloying elements is observed in the film [Figs. 4(e–k)]. It indicates that at the initial stage of oxidation, Al atoms first migrate from single-crystal matrix to the sample surface and react with oxygen to form Al_2O_3, which

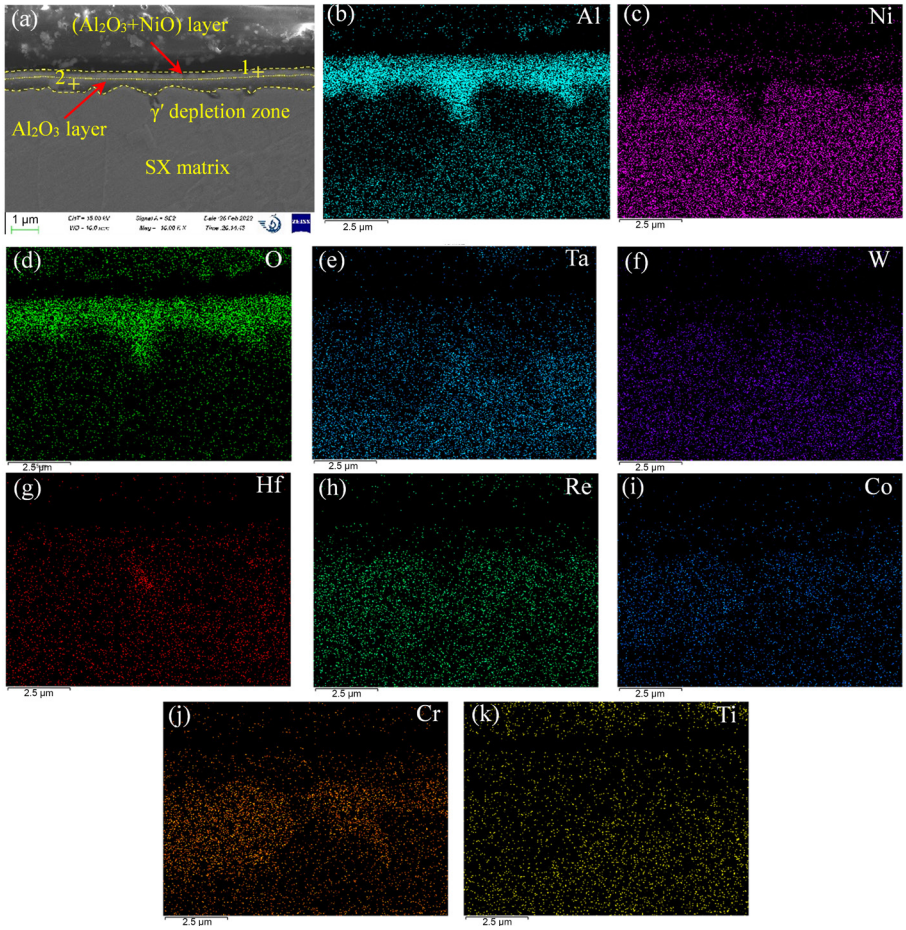

Fig. 4: Microstructure image (a) and EDS mapping results (b–k) of 4774DD1 alloy oxidized at 980 °C for 25 h

Table 2: EDS point analysis results (at.%) of Positions 1 and 2 marked in Fig. 4(a)

Position	O	Al	Ti	Cr	Ni	Co	Hf
1	47.08	34.19	0.64	2.44	12.82	2.83	–
2	57.38	35.70	–	0.81	2.66	–	3.45

is identified by XRD (Fig. 3). At this moment, the Al_2O_3 film is not compact, and cations of Ni^{2+}, Cr^{3+}, Ta^{6+}, as well as oxygen atoms could easily diffuse through the film [11]. Therefore, the Al and Ni atoms diffuse through the Al_2O_3 film and react with oxygen to form a small amount of NiO in the top part of the Al_2O_3 film. At this time, the NiO has a small grain size and mixes with Al_2O_3 film, which can be observed from the distribution of Al and Ni element in the EDS results. Owing to the depletion of Al element by oxidation, a γ′ (Ni_3Al) depletion zone is formed underneath the oxide film.

Figure 5 shows the microstructure and elements mapping of the oxide film of the alloy oxidized at 980 °C for 75 h. Table 3 lists the EDS point analysis results of different positions in Fig 5(a). Figure 5(a) exhibits that the oxide film primarily contains two layers. The outermost layer is composed of discontinuous Ni-rich grains [Fig. 5(c) and Position 6 in Table 3], which is identified as NiO by XRD analysis in Fig. 3. It is consistent with the study of Ref. [22]. The internal layer consists of three sublayers, as shown in Fig. 5(a). The bottom sublayer is continuous and mainly concentrated with Al element [Fig. 5(b) and Position 3 in Table 3]. Combined with XRD analysis, the phase formed in this bottom sublayer is dominantly Al_2O_3. The upper sublayer is continuous and enriched in Al and Ni elements according to Figs. 5(b, c) and Position 5 in Table 3. Combining with XRD analysis, the sublayer contains Al_2O_3 and NiO. Figure 5(a) shows that the intermediate sublayer (enclosed by red dot lines) consists of a continuous substrate and a discontinuous phase. Figures 5(b, e and j) and Position 4 in Table 3 show that Al, Cr and Ta elements concentrate in the intermediate sublayer. Associated with XRD analysis, the continuous substrate is Al_2O_3, while the discontinuous phase is identified as $CrTaO_4$. In comparison to 25 h oxidation, the Al_2O_3+NiO mixed sublayer and Al_2O_3 sublayer become thicker, and the γ′ depletion zone becomes larger.

Figure 6 shows the morphology and EDS mapping analysis of the oxide film oxidized at 980 °C for 125 h. Table 4 lists the EDS point analysis results of different positions in Fig. 6(a). It can be seen from Fig. 6(a) that the oxide film consists of two main layers which is similar to that oxidation for 75 h. The outmost layer is not compact and concentrated with Ni

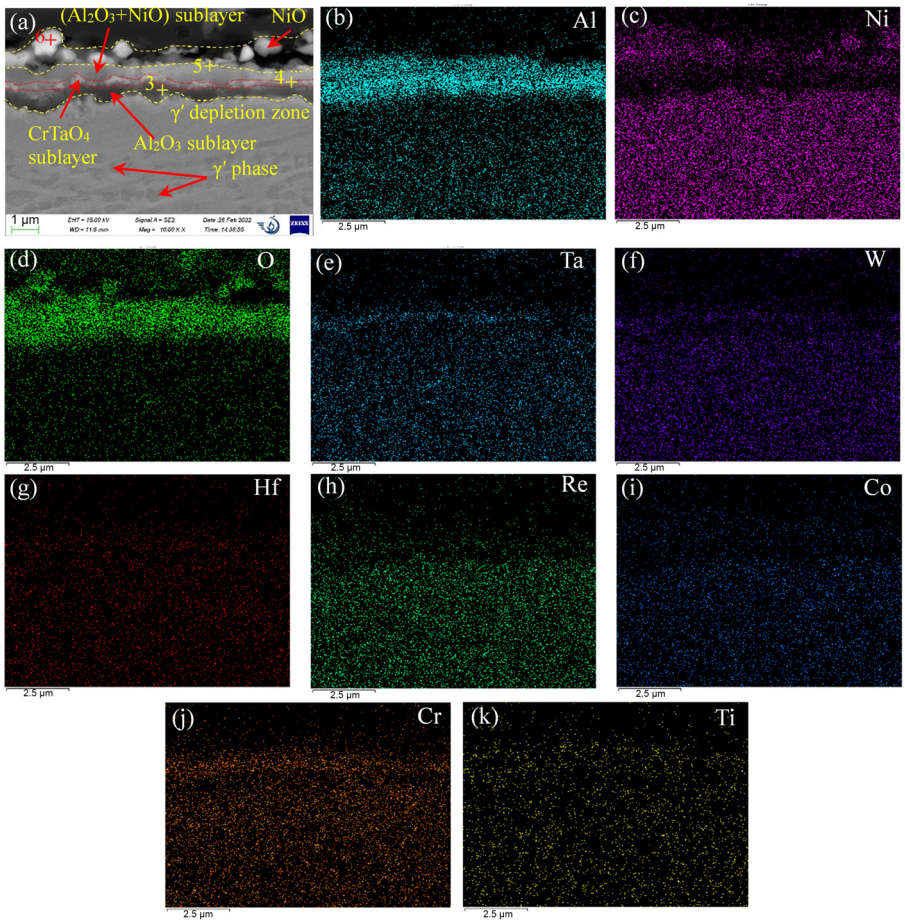

Fig. 5: Microstructure image (a) and EDS mapping results (b–k) of 4774DD1 alloy oxidized at 980 °C for 75 h

Table 3: EDS point analysis results of Positions 3, 4, 5 and 6 marked in Fig. 5(a) (at.%)

Position	O	Al	Ti	Cr	Ni	Co	Ta	W
3	47.03	38.88	–	3.78	8.52	1.79	–	–
4	54.53	18.35	2.35	10.76	4.47	2.47	6.12	0.95
5	47.61	27.26	0.67	7.56	16.90	–	–	–
6	42.85	3.18	–	0.99	52.98	–	–	–

element. Combined with the XRD analysis (Fig. 3), the oxide is identified as NiO which is similar with that oxidized for 75 h. But, the grain size is significantly increased. The internal layer is composed of three sublayers. The bottom sublayer is enriched with Al elements. According to the XRD results in Fig. 3, the phase dominating in the sublayer is Al_2O_3. Compared to the film oxidized for 75 h, this sublayer becomes thicker. The intermediate sublayer (enclosed by red dot lines) exhibits a continuous thin band which is concentrated with Ni, Ta, W and Cr elements, which can be identified as $CrTaO_4$ and $NiWO_4$. The upper sublayer is not compact and aggregated with Al and Ni elements, as shown in Figs. 6 (b, c) and Position 9 in Table 4. This sublayer is primarily consisted of Al_2O_3 and NiO, which is similar to that after 75 h oxidation. But, this sublayer becomes thicker. Since more Al element diffused from single-crystal matrix to the oxide film, the γ′ depletion zone is further enlarged.

Figure 7 shows the microstructure and EDS mapping analysis of the oxide film of the alloy exposured for 200 h. Table 5 lists the EDS point analysis results of different layers of the film marked in Fig. 7(a). It can be seen from Fig. 7(a) that the film contains three layers. The internal layer is mainly enriched with Al elements. Combined with the XRD analysis, the phase in this layer is primarily Al_2O_3. In comparison to the 125 h, little change in the thickness of this layer can be found. The intermediate layer is compact and concentrated with Ni, Ta, W and Cr elements, as shown in Figs. 7(c, e, f and j) and Position 12 in Table 5. When these composition analysis are associated with the XRD analysis in Fig. 3, the phases in the intermediate layer can be identified as mainly the mixture of $CrTaO_4$ and $NiWO_4$. In comparison to the 125 h, this mixture layer becomes obviously thicker. It can be seen from Figs. 7(b, c and j) and Position 13 in Table 5, Al, Ni and Cr elements concentrate in the outermost layer. Combined with the XRD analysis, the oxides in this layer are mainly composed of $NiAl_2O_4$ and $NiCr_2O_4$.

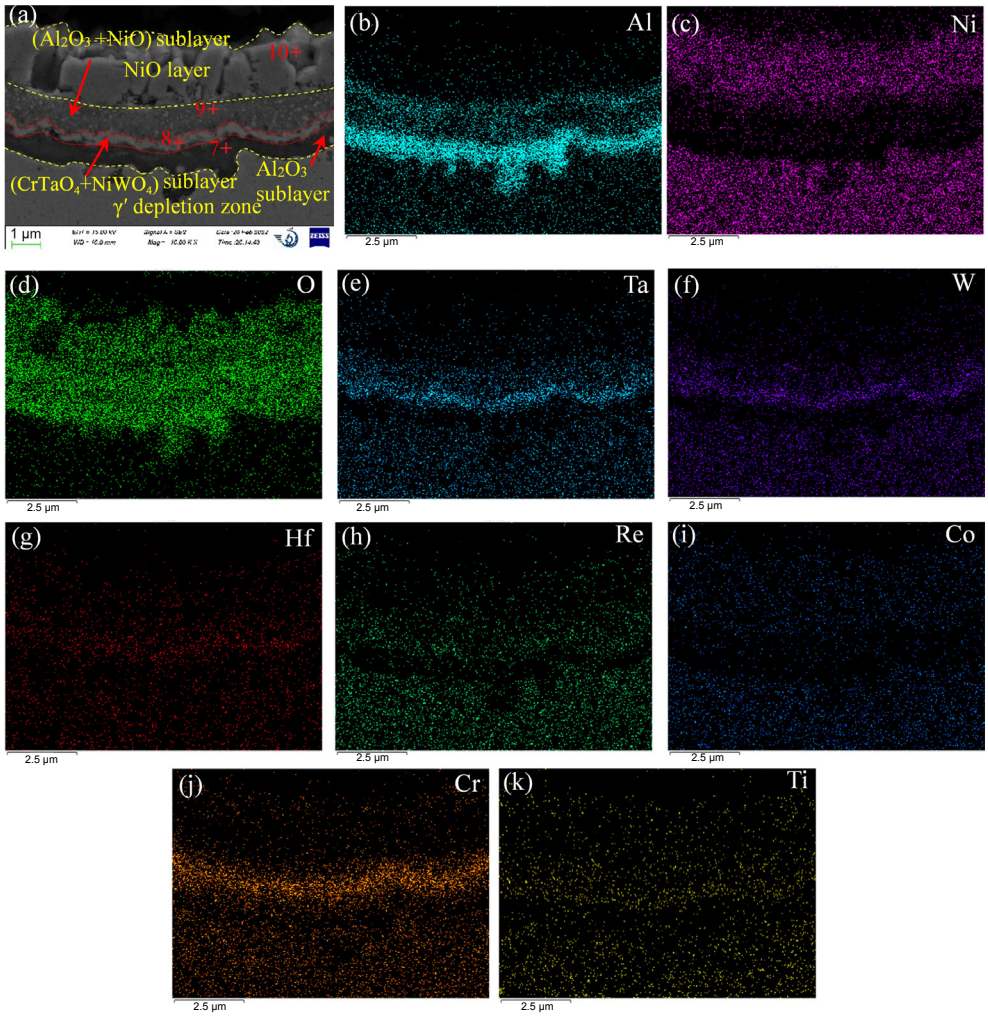

Fig. 6: Microstructure image (a) and EDS mapping results (b–k) of 4774DD1 alloy oxidized at 980 °C for 125 h

Table 4: EDS point analysis results (at.%) of Positions 7, 8, 9 and 10 marked in Fig. 6(a)

Position	O	Al	Ti	Cr	Ni	Co	Ta	W
7	52.61	36.81	0.85	5.95	2.31	–	1.47	–
8	57.75	5.26	6.51	12.64	3.76	–	11.65	2.43
9	57.41	11.57	2.82	7.85	12.92	–	7.43	–
10	41.23	–	–	–	58.77	–	–	–

3.4 Oxidation mechanisms

In terms of the above combination studies of oxidation kinetics, XRD analysis, SEM microstructure, and EDS elements distribution analysis, the oxidation mechanisms of the 4774DD1 Ni-based single-crystal superalloy could be illustrated schematically in Fig. 8. At the beginning of the oxidation, Al atoms would firstly react with oxygen to form Al_2O_3 film because of its higher affinity for oxygen compared to other alloying elements [23]. Since Al is the main forming element of γ′ phase (Ni_3Al), a γ′ depletion zone can be observed beneath the Al_2O_3 film. The Al_2O_3 film is not compact, through which the oxygen and other metal atoms could diffuse inward and outward. Because there is a large amount of Ni element in nickel-based single-crystal, according to the diffusion principle, Ni element will diffuse from single-crystal superalloy matrix with a high concentration to the oxide layer with a low concentration, some Ni atoms migrate outward from single-crystal matrix through bottom part of the Al_2O_3 film to its top part and react with inward diffused oxygen to form NiO grains. Therefore, at this time, the oxidation film is composed of Al_2O_3 sublayer in the bottom part plus (Al_2O_3+NiO) mixture sublayer in the upper part, as illustrated in Fig. 8(a). With the increase of oxidation time, more Al outward diffuses to the oxidation film and reacts with the inward diffused oxygen to form more Al_2O_3, causing a larger depletion zone of the γ′ phase. At the same time, increasing Ni diffuses outward to the upper part of the film and reacts with oxygen to form more NiO there. Hence, the bottom Al_2O_3 sublayer and upper (Al_2O_3+NiO) mixture sublayer become thicker. Meanwhile, some Ni atoms can diffuse out of the internal layer and directly react with oxygen to form NiO

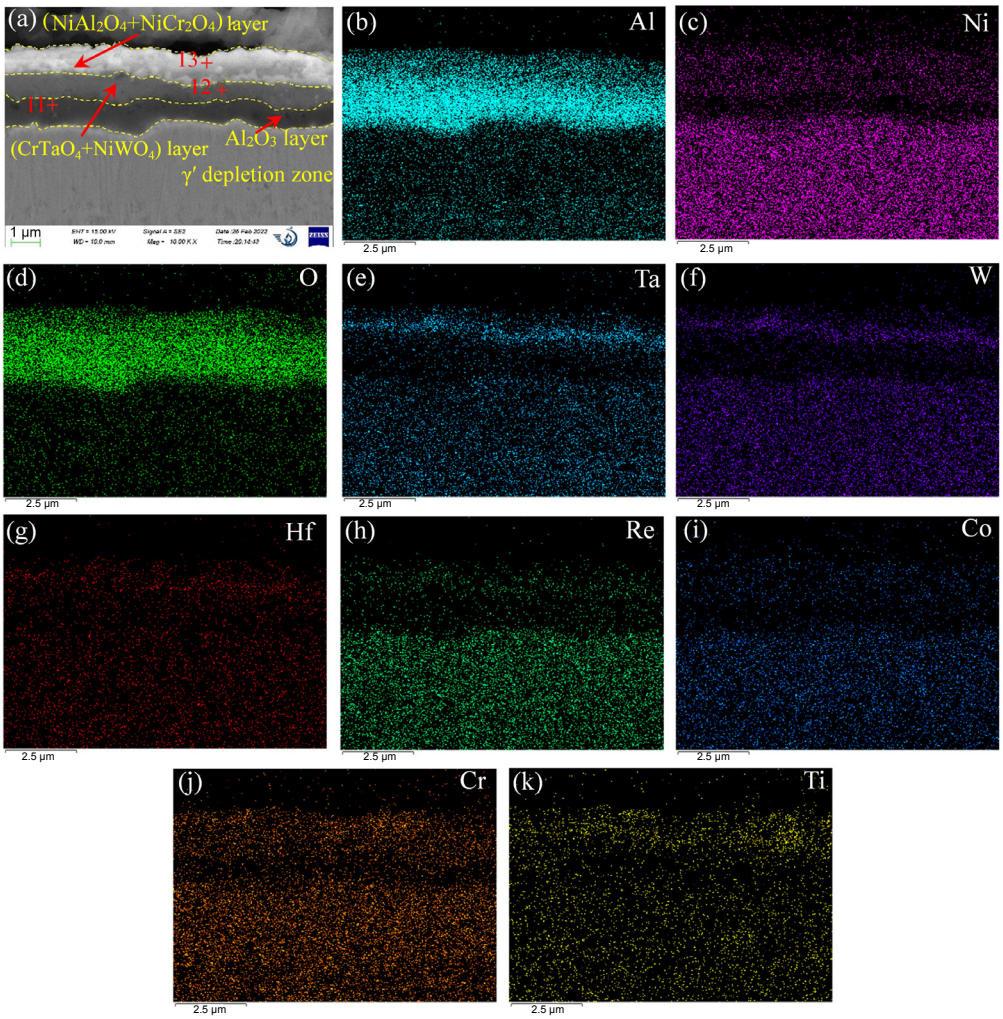

Fig. 7: Microstructure image (a) and EDS mapping results (b–k) of 4774DD1 alloy at 980 °C for 200 h

Table 5: EDS point analysis results (at.%) of Positions 11, 12 and 13 marked in Fig. 7(a)

Position	O	Al	Ti	Cr	Ni	Co	Ta	W
11	51.70	42.46	0.36	2.49	2.40	0.59	–	–
12	51.06	2.20	0.37	14.67	7.10	–	14.90	6.70
13	46.40	23.95	0.30	12.17	17.18	–	–	–

grains on the outermost surface of the samples, as shown in Fig. 8(b). In addition, some Cr and Ta atoms migrate from single-crystal matrix and aggregate in the internal layer. When their quantity exceeds their degree of supersaturation in the internal layer, the $CrTaO_4$ is directly precipitated. Thus, the oxidation film is composed of the outermost small NiO discontinuous grain layer plus internal layer (bottom Al_2O_3 sublayer+intermediate narrow $CrTaO_4$ sublayer+upper (Al_2O_3+NiO) mixture sublayer), as illustrated in Fig. 8(b). When the oxidation time is increased to 125 h, the amount of Ni atoms diffusing through the internal layer to the outmost layer increases. This results in a relative continuous NiO layer with large grain size. Due to that the Al and Ni atoms migrate from single-crystal matrix to the internal layer, the upper (Al_2O_3+NiO) mixture sublayer becomes thicker, the bottom Al_2O_3 sublayer becomes compact, and the γ′ depletion zone becomes larger than that after 75 h oxidation. Furthermore, more Cr, Ta and W move into the internal layer, which leads to the formation of continuous ($CrTaO_4$+$NiWO_4$) mixture sublayer. Therefore, at this moment the oxide film is composed of the outermost relative continuous NiO layer with large grain size and internal layer which consists of upper (Al_2O_3+NiO) mixture sublayer, intermediate continuous ($CrTaO_4$+$NiWO_4$) mixture sublayer and bottom Al_2O_3 sublayer, as shown in Fig. 8(c). With further increasing oxidation time to 200 h, the ($CrTaO_4$+$NiWO_4$) mixture layer becomes thicker because more Cr, Ta, W and Ni migrate into the oxidation film. Meanwhile, the outermost NiO layer is transformed to ($NiAl_2O_4$+$NiCr_2O_4$) mixture layer which might be formed through the following reactions:

$$NiO + 2Cr + 3/2O_2 = NiCr_2O_4 \quad (4)$$

$$NiO + 2Al + 2O_2 = NiAl_2O_4 \quad (5)$$

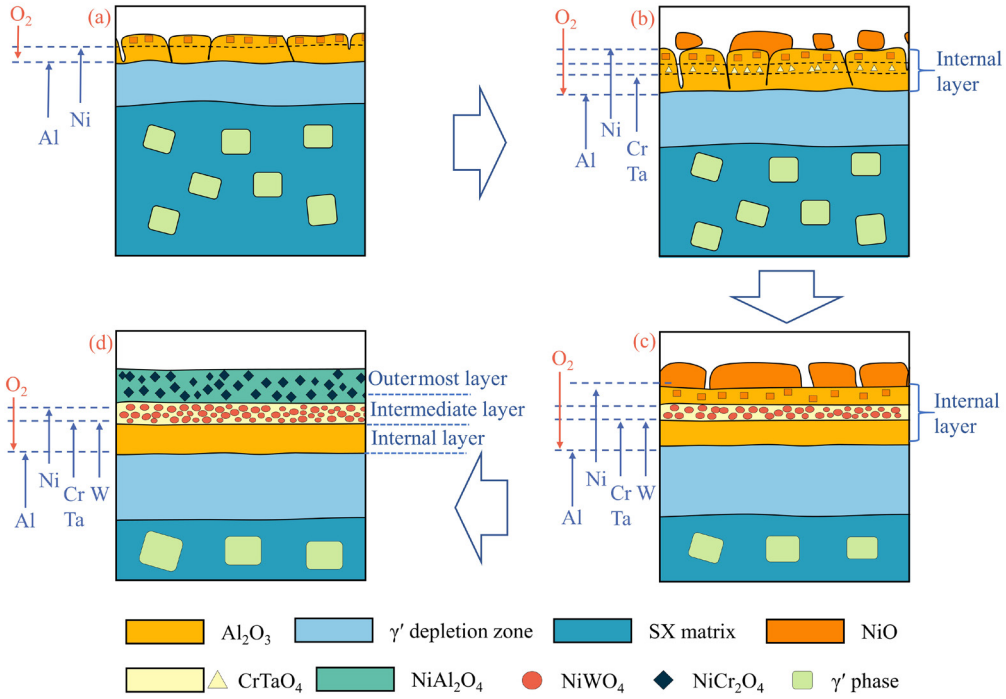

Fig. 8: Schematic illustration of oxidation film evolution of 4774DD1 alloy oxidized at 980 °C for different times: (a) 25 h; (b) 75 h; (c) 125 h; (d) 200 h

Hence, after 200 h oxidation, the oxide film consists of the outermost ($NiAl_2O_4$+$NiCr_2O_4$) mixture layer, intermediate ($CrTaO_4$+$NiWO_4$) mixture layer, and bottom Al_2O_3 layer, as shown in Fig. 8(d). Due to little Al atoms move into the bottom Al_2O_3 layer compared to that oxidized for 125 h, the thickness of the Al_2O_3 layer and the size of γ′ depletion zone change inconspicuously as the oxidation time extends to 200 h.

4 Conclusions

The isothermal oxidation behavior of 4774DD1 single-crystal Ni-based superalloy at 980 °C was investigated. The following conclusions are drawn:

(1) The oxidation kinetics of the experimental alloy obey the cubic law, and the alloy exhibits a certain oxidation-resistance at 980 °C, which can meet the requirement of industrial gas turbine single-crystal blades.

(2) At 980 °C, the morphologies of oxide film evolve from one layer to two layers and ultimately become three layers with the extension of oxidation time.

(3) The initial oxide scale on the surface of 4774DD1 consists of Al_2O_3 and NiO. As the oxidation progresses, $CrTaO_4$, $NiWO_4$, $NiAl_2O_4$ and $NiCr_2O_4$ spinels are formed in the oxide film due to continuous migration of Cr, Ta, Ni, and W elements during the oxidation process.

(4) The γ′ depletion zone is formed beneath the oxide film due to the consumption of Al and Ni elements in the alloy matrix when the oxidation time exceeds 75 h. However, there is minimal change observed in the size of the γ′ depletion zone when oxidation time extends to 125 h, as the migration of Al and Ni elements is impeded by a dense layer of Al_2O_3.

Acknowledgments

This work was supported by the fund of State Key Laboratory of Long-life High Temperature Materials (Grant No. DTCC28EE200787), the Natural Science Basic Research Plan in Shaanxi Province of China (Grant No. 2022JQ-553), the China Postdoctoral Science Foundation (Grant No. 2021M692555), the Excellent Youth Foundation of Shaanxi Province of China (Grant No. 2021JC-08), and the Beilin district of Xi'an Science and Technology Project (Grant No. GX2123). The authors would like to acknowledge the support from the Youth Innovation Team of Shaanxi Universities.

Conflict of interest

The authors declare that they have no known competing financial interests or personal relationships that could have appeared to influence the work reported in this paper.

References

[1] Chen J, Huo Q, Chen J, et al. Tailoring the creep properties of second-generation Ni-based single crystal superalloys by composition optimization of Mo, W and Ti. Materials Science and Engineering: A, 2021, 799: 140163.

[2] Shang Z, Wei X, Song D, et al. Microstructure and mechanical properties of a new nickel-based single crystal superalloy. Journal of Materials Research and Technology, 2020, 9(5): 11641–11649.

[3] Zhang H, Li P, Gong X, et al. Tensile properties, strain rate sensitivity and failure mechanism of single crystal superalloys CMSX-4. Materials Science and Engineering: A, 2020, 782: 139105.

[4] Hao X, Liu G H, Wang Y, et al. Optimization of investment casting process for K477 superalloy aero-engine turbine nozzle by simulation and experiment. China Foundry, 2022, 19(4): 351–358.
[5] Hino T, Kobayashi T, Koizumi Y, et al. Development of a new single crystal superalloy for industrial gas turbines. Superalloys, 2000, 1(1): 729–736.
[6] Sato A, Moverare J J, Hasselqvist M, et al. On the mechanical behavior of a new single-crystal superalloy for industrial gas turbine applications. Metallurgical and Materials Transactions: A, 2012, 43: 2302–2315.
[7] Jahns K, Lai H, Krupp U, et al. On oxide formation on a single crystalline Ni-based superalloy at 900 °C in SO_2 containing atmosphere: The effect of surface treatment. Corrosion Science, 2021, 180: 109154.
[8] Evangelou A, Soady K A, Lockyer S, et al. On the mechanism of oxidation-fatigue damage at intermediate temperatures in a single crystal Ni-based superalloy. Materials Science and Engineering: A, 2019, 742: 648–661.
[9] Cervellon A, Hémery S, Kürnsteiner P, et al. Crack initiation mechanisms during very high cycle fatigue of Ni-based single crystal superalloys at high temperature. Acta Materialia, 2020, 188: 131–144.
[10] Li X, Liu Y, Zhao Y, et al. Oxygen changes crack modes of Ni-based single crystal superalloy. Materials Research Letters, 2021, 9(12): 531–539.
[11] Pei H, Wen Z, Yue Z. Long-term oxidation behavior and mechanism of DD6 Ni-based single crystal superalloy at 1,050 °C and 1,100 °C in air. Journal of Alloys and Compounds, 2017, 704: 218–226.
[12] Zhou X F, Chen G, Feng Y Y, et al. Isothermal oxidation behavior of a new Re-free nickel-based single-crystal superalloy at 950 °C. Rare Metals, 2017, 36: 617–621.
[13] Shi Z, Li J, Liu S. Isothermal oxidation behavior of single crystal superalloy DD6. Transactions of Nonferrous Metals Society of China, 2012, 22(3): 534–538.
[14] Liu C T, Ma J, Sun X F. Oxidation behavior of a single-crystal Ni-base superalloy between 900 and 1,000 °C in air. Journal of Alloys and Compounds, 2010, 491(1–2): 522–526.
[15] Hu Y, Cao T, Cheng C, et al. Oxidation behavior of a single-crystal Ni-based superalloy over the temperature range of 850 °C–950 °C in air. Applied Surface Science, 2019, 484: 209–218.
[16] Li M, Wang P, Yang Y Q, et al. Oxidation behavior of a nickel-based single crystal superalloy at 1,100 °C under different oxygen concentration. Journal of Materials Science, 2022, 57(5): 3822–3841.
[17] Hu Y, Cheng C, Zhang L, et al. Microstructural evolution of oxidation film on a single crystal nickel-based superalloy at 980 °C. Oxidation of Metals, 2018, 89: 303–317.
[18] Li P, Jin X, Zhao J, et al. Oxidation behaviors and compressive strength evolution of DD6 Ni-based single-crystal superalloy at 1,100 °C. Corrosion Science, 2022, 208: 110684.
[19] Wu Y, Narita T. Oxidation behavior of the single crystal Ni-based superalloy at 900° C in air and water vapor. Surface and Coatings Technology, 2007, 202(1): 140–145.
[20] Tan Z H, Wang X G, Song W, et al. Oxidation behavior of a novel nickel-based single crystal superalloy at elevated temperature. Vacuum, 2020, 175: 109284.
[21] Wang M, Cheng X, Jiang W, et al. The effect of amorphous coating on high temperature oxidation resistance of Ni-based single crystal superalloy. Corrosion Science, 2023, 213: 111000.
[22] Akhtar A, Hegde S, Reed R C. The oxidation of single-crystal nickel-based superalloys. JOM, 2006, 58: 37–42.
[23] Mrowec S. On the mechanism of high temperature oxidation of metals and alloys. Corrosion Science, 1967, 7(9): 563–578.